HHS Public Access

Author manuscript

Arthritis Rheumatol. Author manuscript; available in PMC 2021 February 01.

Published in final edited form as:

Arthritis Rheumatol. 2020 February ; 72(2): 316–325. doi:10.1002/art.41085.

Using transitional changes on HRCT to monitor the impact of cyclophosphamide or mycophenolate on systemic sclerosis-related interstitial lung disease

Grace Hyun J. Kim, PhD, MS,
Department of Radiological Sciences, David Geffen School of Medicine at UCLA, Department of Biostatistics, Fielding School of Public Heath, Los Angeles, California

Donald P. Tashkin, MD,
Division of Pulmonary and Critical Care Medicine, Department of Medicine David Geffen School of Medicine at UCLA, Los Angeles, California

Pechin Lo, PhD,
Department of Radiological Sciences, David Geffen School of Medicine at UCLA, Los Angeles, California

Matthew S. Brown, PhD,
Department of Radiological Sciences, David Geffen School of Medicine at UCLA, Los Angeles, California

Elizabeth R. Volkmann, MD, MS,
Division of Rheumatology, Department of Medicine, David Geffen School of Medicine at UCLA, Los Angeles, California

David W. Gjertson, PhD, MS,
Department of Biostatistics, Fielding School of Public Heath, Los Angeles, California

Dinesh Khanna, MD, MS,
Division of Rheumatology, Department of Internal Medicine, University of Michigan, Ann Arbor, Michigan

Robert M. Elashoff, PhD,
Department of Biomathematics, David Geffen School of Medicine at UCLA, Los Angeles, California

Chi-Hong Tseng, PhD,
Statistics Core, Division of General Internal Medicine and Health Services Research, Department of Medicine, David Geffen School of Medicine at UCLA, Los Angeles, California

Michael D Roth, MD,
Division of Pulmonary and Critical Care Medicine, Department of Medicine David Geffen School of Medicine at UCLA, Los Angeles, California

Correspondences: Grace Hyun j. Kim, Address: Department of Radiological Science, David Geffen School of Medicine at UCLA, 10833 Le Conte Ave, Los Angeles, CA 90095; Telephone number: 310-481-7594, Fax number: 310-794-8657, gracekim@mednet.ucla.edu.

Jonathan G Goldin, MD PhD
Department of Radiological Sciences, David Geffen School of Medicine at UCLA

Abstract

OBJECTIVE: To examine changes in the extent of specific patterns of interstitial lung disease (ILD) as they transition from one pattern to another in response to immunosuppressive therapy of Systemic Sclerosis-related ILD. (SSc-ILD)

METHODS: We evaluated changes in the quantitative extent of specific lung patterns of ILD using volumetric HRCT scans obtained at baseline and 2 years after therapy in patients treated with either cyclophosphamide (CYC) for 1 year or mycophenolate (MMF) for 2 years in the Scleroderma Lung Study II. ILD patterns included: lung fibrosis (LF), ground glass (GG), honeycombing (HC), and normal lung (NL). Net changes were calculated as the differences in the probabilities of changes from one ILD pattern to another. Wilcoxon signed-ranks tests were used to compare the changes.

RESULTS: Forty-seven and 50 patients had baseline and follow-up scans in the CYC and MMF arms, respectively. Mean net improvements reflecting favorable changes in extent of ILD from one pattern to another in the whole lung in the CYC and MMF groups, respectively, were as follows: from LF to NL (21% and 19%), from GG to NL (30% and 28%) and from LF to GG (5% and −0.6%). Means of overall improvement in transitioning from GG or LF to NL patterns were significant for both treatments (all $p<0.001$).

CONCLUSIONS: Significantly favorable transitions from both GG and LF ILD patterns to NL were found in patients undergoing immunosuppressive treatment for SSc-ILD, suggesting the usefulness of examining these transitions for insights into the underlying pathobiology of treatment response.

TRIAL REGISTRY: ClinicalTrials.gov; No.: ;

Keywords

Quantitative Fibrosis; Classification; Transition; Interstitial Lung Disease

INTRODUCTION

Systemic sclerosis (scleroderma, SSc) is a complex life-threatening autoimmune disease associated with tissue fibrosis. SSc-related interstitial lung diseases (SSc-ILD) is common and is the leading cause of mortality in SSc [1–3]. The majority of patients with SSc develop parenchymal abnormalities on high-resolution chest computed tomography (HRCT), while only approximately 40% develop significant ventilatory restriction (forced vital capacity [FVC] below 75% of predicted) and 10–15% develop severe restrictive abnormality (FVC<50% predicted)[3,4]. Most SSc patients develop ILD within the first 5–10 years of disease onset and those with more severe restrictive abnormality are at greatest risk of progression to respiratory failure and death[5]).

HRCT alterations characteristic of SSc-ILD include reticulations with architectural distortion (representing fibrosis), ground glass opacity (GGO) defined as opacity through

which normal lung markings may be visualized, representing either inflammation and/or early fibrosis and, to a lesser extent, honeycombing (cystic air spaces with fibrous walls)[6]. The combination of these elements represents the total burden of interstitial lung disease (ILD) that can broadly be assessed either visually or quantitatively using image analysis software[6–15]. Along with pulmonary function tests, the radiographic extent of disease in patients with SSc-ILD is important for diagnosis, the staging of disease severity, and the assessment of changes during follow-up[16,17]. Furthermore, changes in the extent of fibrosis (reticulations) assessed in the whole lung or in the most involved lobes either visually or by computer-aided quantitative analysis occur in parallel with changes in pulmonary function tests in response to treatment with oral cyclophosphamide or placebo over a one-year period.

We previously reported transitional changes in the pixel-based quantitative extent of disease from one ILD pattern to another from paired HRCT scans obtained one year apart in 83 patients with SSc-ILD who participated in a trial of oral cyclophosphamide (CYC; n=41) versus placebo (n=42) administered for one year (Scleroderma Lung Study I [SLS I]) [21]. We found significantly greater changes over the one-year course of the study from a fibrotic or a ground glass pattern to a normal pattern than the reverse in the 41 CYC-treated patients, whereas the placebo-treated patients tended to show changes in the opposite direction. A limitation of this prior study was that the scans were non-volumetric and were based on matching arbitrarily designated zones, thereby precluding the ability to quantitate the extent of ILD based on matching voxels and to segment the lung into lobes for analysis of voxel-wise transitions within specific lobes.

To further explore transitional changes in the HRCT patterns of SSc-ILD as a sensitive and specific metric of disease progression and treatment response in patients with SSc-ILD, we now present the results of individual voxel-wise changes over two years in HRCT patterns of quantitative lung fibrosis (QLF), quantitative ground glass opacity (QGG), and quantitative normal lung (QNL) in both the whole lung and the most severely affected lobe in participants in Scleroderma Lung Study II (SLS II), a multi-center trial of oral CYC versus mycophenolate mofetil (MMF) in patients with symptomatic SSc-ILD [22].

MATERIALS AND METHODS

Patient Selection

Ninety-seven patients with symptomatic SSc-ILD (25 males, 72 females, with a mean (±SD) forced vital capacity (FVC) of 66.3% (8.9 %) predicted and diffusing capacity for carbon monoxide (DL_{CO}) of 55.0% (13.1%) predicted, who participated in the 14-center SLS II and successfully underwent HRCT scans at screening (“baseline”) and 2 years following randomization were evaluated for the purpose of this exploratory outcome analysis. Eligible participants were randomly assigned to receive, in a double-blind fashion, either oral CYC (titrated up to 2 mg/kg per day, as tolerated) for one year followed by placebo for an additional year or MMF (titrated to 1500 mg twice daily, as tolerated) for 2 years. This research was approved by an Institutional Review Board (IRB). Full details concerning the SLS II methodology, including eligibility criteria, have been reported previously [22].

Measurements of FVC, $DL_{CO,}$ total lung capacity (TLC), dyspnea (Mahler baseline dyspnea index [BDI] and transition dyspnea index [TDI]) (23) and skin thickness score (modified Rodman skin score [mRSS]) (24) were performed at baseline and repeated every 3 months (FVC, DL_{CO}, mRSS) or every 6 months (TLC and TDI) for 2 years[23,24]. The study was approved by the local institutional review board of each participating institution. All radiographic image management was compliant with the Health Insurance Portability and Accountability Act.

CT Scanning Protocol

HRCT was used to scan patients at maximal inspiration. Images were acquired from 12 different multi-detector CT scanner models from 2 manufacturers using a standardized protocol following strict quality control protocols. Most patients were scanned at suspended TLC in the prone position (N=92 both visits, N=4 supine at baseline and prone at 24 month or vice versa, and N=1 supine position at both visits). Tube currents ranged from 80 to 100 effective mAs at 120 kVp. Volumetric CT scans of 1–1.50 mm slice thickness were acquired and reconstructed with sharp or over-enhancing filters. Ninety of paired baseline and follow-up scans were acquired using the same CT scanner model.

Quantitative HRCT Image Analyses

Quantitative CT Image Analysis—Whole lung and individual lobes on HRCT images were segmented semi-automatically using an in-house analysis workstation[26]. Visual confirmation of lobar segmentation results was performed by a thoracic radiologist.

Probability of changes in CT scores for extent of ILD abnormality during transition from one to another pattern of ILD—Quantitative CT texture-based scores of disease extent were derived from a supervised texture-based classification model[13]. A multi-step process was used for generating voxel-wise quantitative transitional probabilities from 97 paired HRCT scans: (1) classifying ILD patterns using a Computer Aided Diagnosis (CAD) system that automatically processes and reduces HRCT image noise; calculating the texture features; running the support vector machine model[13]; (2) registering (superimposing) the lobes and each lung between baseline and 24 months [26]; (3) mapping each voxel ($<27mm^3$) using a nearest neighbor algorithm; (4) counting the voxels within each mutually exclusive pattern of ILD (fibrosis, GG, honeycombing, normal) at baseline and 24 months; and calculating a transitional probability (See Supplementary Figure 1 and formulae for details of registration and transitional probability, respectively). A transitional probability is an expression of the probability of changing from one radiographic pattern of ILD to another or remaining the same pattern, and is expressed as a proportion in which the numerator consists of the number of voxels representing a particular pattern of ILD that changes to another pattern (for example, fibrotic pattern [LF] to a normal [NL] pattern) within a given region (whole lung or maximally involved lobe) between baseline and 24 months; the denominator comprises the total number of voxels within the initial pattern at baseline. The probability of stability is the proportion of the number of voxels remaining as the same pattern at 24 months compared to baseline. A Markov transitional matrix schema was used to illustrate the probabilities of changes from one ILD pattern to another within the whole lung or the most severely affected lobe [27].

Four types of quantitative CT CAD patterns were computed: QLF, comprising a fibrotic reticulation pattern only; QHC, comprising a honeycomb pattern; QGG, comprising a ground glass pattern; and QNL, representing a normal lung patterns. Since only 2 of the 97 patients had a QHC score >0 (one of 1.9% and the other of 5.3%) at baseline and the transitional probability of changing from a honeycomb pattern to another pattern was zero, changes in a QHC pattern were omitted for simplicity and the two subjects with non-zero QHC scores were included in the QLF pattern under the assumption that honeycomb might represent a severe form of fibrosis.

An example of a transitional probability from a LF to a GG pattern is as follows:

$$P_{LF \text{ at baseline} \rightarrow GG \text{ at follow-up}} = \frac{counts\ of\ voxels\ that\ convert\ from\ LF\ to\ GG\ patterns}{total\ \ number\ of\ voxels\ \ classified\ as\ LF\ at\ baseline}$$

A stable voxel-wise pattern was represented as $P_{NL\rightarrow NL,}$ $P_{GG\rightarrow GG,}$ or $P_{LF\rightarrow LF}$, indicating the probability of a normal, ground glass or fibrotic pattern remaining the same over 2 years. A transitional net-improvement was defined as the difference in two probabilities, in which the probability of a transition representing worsening (e.g., a GG pattern transitioning to a fibrotic pattern) is subtracted from a probability of a transition representing improvement (e.g., a fibrotic pattern changing to a ground glass pattern). Three net improvements were: $P_{GG\rightarrow NL} - P_{NL\rightarrow GG}$; $P_{LF \rightarrow NL} - P_{NL\rightarrow LF}$; and $P_{LF\rightarrow GG} - P_{GG\rightarrow LF.}$

Statistical Analysis: Descriptive summary statistics were used for reporting demographic and clinical characteristics, pulmonary function measures, and quantitative CT texture scores at baseline and follow-up. CT scores are reported both for the whole lung and for the most severely affected lobe (the lobe with most extent of disease by QLF score at baseline) [20]. We set up a 3X3 matrix consisting of the following transitions: diagonal elements ($P_{NL\rightarrow NL,}$ $P_{GG\rightarrow GG,}$ or $P_{LF\rightarrow LF}$) representing stability; and off-diagonals ($P_{LF\rightarrow GG}$, $P_{GG\rightarrow LF}$, $P_{GG\rightarrow NL}$, $P_{NL\rightarrow GG}$, $P_{LF\rightarrow NL}$, and $P_{NL\rightarrow LF}$), representing transitional changes (for details, see Figures 1 B and D). Net improvement between patterns is represented by the difference between two probabilities, e.g., the probability of transitioning from LF to NL minus the probability of the directionally opposite transition, i.e., from NL to LF ($P_{LF\rightarrow NL} - P_{NL\rightarrow LF}$). After normality checks on a given metric, the Wilcoxon signed-rank test was performed to test for the significance of net improvement from baseline (e.g., $P_{GG\rightarrow LF}$ vs. $P_{LF\rightarrow GG}$: difference in proportions between opposite directional patterns) for the CYC and MMF groups separately. Spearman rank correlations were used to test associations between changes in CT proportions in the whole lung and the most severely affected lobe and absolute changes in percent predicted pulmonary function test parameters. Linear regressions were used to determine the association of baseline demographic and clinical factors with the net benefit of change from ILD patterns of GG to NL and of LF to NL. Backward selection methods were used with the covariates of age, gender, duration of disease, pulmonary function, skin score, and dyspnea scores. A responder analysis was performed using +3% and −3.3% absolute changes in FVC % predicted as the thresholds for defining responders and non-responders, respectively. These thresholds represent previously published findings for the minimal clinically important differences (MCIDs) for absolute changes in FVC% predicted anchored to health related outcomes [28]. Analysis of Variance

(ANOVA) tests were used to compare the net improvements between responder, stable, and non-responder groups.

RESULTS

Baseline characteristics

Baseline demographic, lung function, clinical and quantitative radiographic characteristics (extent of fibrosis and total ILD in the whole lung and the lobe of maximal involvement) are shown in Supplementary Table 1. Patients were predominantly females (74% (72/97)), were mostly middle-aged (mean ± SD: 52 ± 9 years), had ,on average, moderate restrictive ventilatory and diffusion impairment (mean ± SD: 66% ± 9% predicted FVC and 55% ±13% predicted DLCO, respectively), a moderate level of breathlessness (mean ± SD: 7.5± 2.3 Baseline Dyspnea Index score), a mean (± SD) modified Rodnan Skin Score of 14 (± 10), and a mean (± SD) 23% (±21%) extent of fibrosis and 50% (± 22%) extent of total ILD (fibrosis + GG + HC) in the most severely involved lobe.

Transitional Proportion Change

Mean (±SD) duration between the baseline and follow-up CT scans was 24.6 (1.9) months. Figure 1 depicts an example of paired HRCT scans and overlaid images of quantitative patterns with two transitional matrices, one for the whole lung and the other for the most severely affected lobe (as defined by the maximally involved lobe at baseline).

Means of transitional probabilities for changes in each normal or ILD pattern (normal lung, ground glass, and lung fibrosis) to another pattern (e.g., from NL to GG; $P_{NL\rightarrow GG}$) or for remaining in the same pattern (e.g., from NL to NL; $P_{NL\rightarrow NL}$) for the whole lung and the most severely affected lobe are shown in Table 1 by treatment arm. No significant change in transitional probabilities of ILD patterns between two treatment arms (p=0.52 for whole lung and p=0.47 for the most severely affected lobe). Net improvements in GG and fibrotic reticulation (LF) patterns, determined by subtracting unfavorable transitional probabilities (e.g., $P_{GG\rightarrow LF}$) from favorable ones (e.g., $P_{LF\rightarrow GG}$), are shown (e.g., $P_{LF\rightarrow GG} - P_{GG\rightarrow LF}$) in Table 2. For the CYC group in the whole lung, mean transitional probabilities were as follows: 15% from fibrotic reticulation (LF) to GG ($P_{LF\rightarrow GG}$) and 10% from GG to fibrotic reticulation ($P_{GG\rightarrow LF}$) (Table 1), resulting in a net improvement ($P_{LF\rightarrow GG} - P_{GG\rightarrow LF}$) of 5% (Table 2); 25% from fibrotic reticulation to a normal pattern ($P_{LF\rightarrow NL}$), and 4% from a normal to a fibrotic pattern ($P_{NL\rightarrow LF}$) (Table 1) with a net improvement ($P_{LF\rightarrow NL} - P_{NL\rightarrow LF}$) of 21% (Table 2); and 40% from GG to normal ($P_{GG\rightarrow NL}$) and 10% from NL to GG ($P_{NL\rightarrow GG}$) (Table 1) with a net improvement ($P_{GG\rightarrow NL} - P_{NL\rightarrow GG}$) of 30% (Table 2). For the MMF group in the whole lung, the net improvements were ~0.00%, 19%, and 28% between fibrotic reticulation and GG ($P_{LF\rightarrow GG} - P_{GG\rightarrow LF}$), between reticulation and a normal pattern ($P_{LF\rightarrow NL} - P_{LF\rightarrow NL}$), and between GG and a normal pattern ($P_{GG\rightarrow NL} - P_{NL\rightarrow GG}$), respectively. Similar mean transitions were found in the most severely affected lobe (Table 1, bottom panel). The net improvements (or lack thereof) in the mean probabilities for these transitional changes for each treatment arm separately and combined are also illustrated by box-whisker plots in Figure 2 and by the Markov transition chain schema in Figure 3. The findings demonstrate the mean net improvements in transitions

from both lung fibrosis and ground glass to a normal pattern in both treatment arms, but essentially no significant net improvement in transitions from lung fibrosis to ground glass.

Table 3 describes the associations between quantitative CT changes (from baseline to 24-month follow-up) and both (1) baseline demographic and clinical/radiographic characteristics and (2) changes in clinical outcomes of lung function, dyspnea and skin score over the same time period. The clinical factors that were significantly associated with improvement in GG to NL patterns were high scores on BDI (less baseline dyspnea) and female gender (adjusted R^2 =0.10). Baseline clinical factors associated with favorable transitions form LF to NL were less restrictive ventilatory impairment (less reduction in FVC), high (worse) skin scores, and female gender (adjusted R^2 =0.16).

Associations of transitional changes in ILD patterns with changes in relevant clinical features over 24 months are shown in the bottom portion of Table 3. The net improvements between GG and NL and between fibrotic reticulation and GG showed statistically significant correlations with all PFT measurements (% predicted FVC, DLCO and TLC) in both the whole lung and the most severely affected lobe, while improvement from a fibrotic pattern to a normal pattern was significantly associated with improvements in FVC and TLC in the whole lung only. Net improvements in fibrotic reticulation to both normal and GG patterns in both the whole lung and the most severely affected lobe were also significantly correlated with favorable changes in skin score but not with the TDI. The net improvements between fibrotic reticulation and GG and between fibrotic reticulation and NL showed statistically significant correlations with changes in skin scores in both the whole lung and the most severe lobe, whereas no significant associations were found between the radiological net improvement and changes in dyspnea.

A responder analysis was also performed to assess whether favorable transitional changes in ILD patterns were associated with clinically meaningful changes in FVC% predicted using previously published values for minimal clinically meaningful differences (MCID) in FVC% predicted over a one-year time period. Results of this analysis are shown in Supplementary Table 3. Favorable transitional changes were uniformly greater in the responder and stable groups than the non-responder group, and differences across groups were statistically significant except for the transition from LF to NL in the most severely affected lobe.

DISCUSSION

Treatment with either CYC for one year followed by placebo for an additional year or MMF for two years was associated with comparably significant increases in the probabilities of a net improvement from both ground glass and fibrotic patterns of ILD to a normal lung pattern. Moreover, these favorable radiographic changes in the whole lung were associated with improvements in FVC and TLC, while the net improvement from a ground glass to a normal pattern in both the whole lung and the most severely affected lobe was associated with improvements in DLCO, FVC and TLC. In addition, significant associations were found between the net improvement in fibrotic patterns and reduction in skin severity. These findings demonstrate that treatment-related improvements in structural patterns of ILD within the lung are accompaniedby parallel improvements in lung function, as well as in

extra-pulmonary (cutaneous) involvement. Finally, transitional changes from GG to NL, LF to GG and LF to NL were associated with minimal clinically important changes in FVC % predicted that define either a positive response to immunosuppressive therapy or at least stable lung function.

Although specific baseline characteristics were significantly associated with favorable transitions from GG to NL (less dyspnea and female gender) or from LF to NL (less restriction, worse skin scores and female gender), these associations, while statistically significant, were not strong (adjusted R^2 0.10 to 0.16), underscoring the importance of clinical monitoring, including serial lung function measurements along with judicious radiographic imaging.

This study provides further evidence that serial HRCT scans play an important and confirmatory role in monitoring the course of SSc-ILD. Patients with newly diagnosed SSc routinely undergo an initial HRCT scan as part of the assessment for the presence or absence of associated ILD with subsequent monitoring of lung function for evidence of the development or worsening of ILD[29]. Follow-up HRCT scans may be warranted to confirm the development or worsening of ILD suggested by changes in lung function, given the variability and non-specificity of lung function measurements (which can be influenced by technical factors and/or inadequate patient effort [30,31]), in contrast to structural changes on HRCT that are more sensitive and specific indicators of parenchymal lung disease. The combination of lung function measurements and extent of ILD on HRCT has been suggested as a guide to decision-making regarding the initiation of disease-modifying therapy for SSc-ILD [32]. Continued monitoring of patients with established SSc-ILD already on immunosuppressive therapy with serial assessments of lung function and symptoms (e.g., dyspnea and cough) may reveal equivocal findings (e.g., disparity between changes in lung function and dyspnea or between changes in FVC and DLCO suggestive of pulmonary hypertension [33]) that might require performance of a follow-up HRCT scan for definitive assessment regarding whether or not the ILD has progressed, in which case a modification of the therapeutic regimen might be indicated. A recent publication of serial changes in lung function performed at 3-month intervals and follow-up HRCT scans in participants in Scleroderma Lung Study II provides some examples of patients with disparate changes in lung function and HRCT scans [34]. Assessing the direction and magnitude of the quantitative voxel-wise changes from one HRCT pattern of ILD to another represents a novel method of demonstrating the efficacy of treatment for SSc-ILD. This approach provides information on dynamic changes in the specific elements of structural abnormality of ILD patterns in the lung in response to treatment. This is both complementary to and more directly related to changes in abnormalities in lung structure than is the measurement of changes in lung function alone.

Interestingly, the net improvements in response to therapy that we noted were mainly from a fibrotic or a ground glass pattern to a normal pattern, not from a fibrotic to a ground glass pattern. While the pathobiology of ground glass opacity in SSc-ILD is not clear (e.g., whether it represents inflammatory changes in the lung or early fibrosis), it is plausible that lung inflammation in SSc-ILD may be a precursor to fibrosis as the disease progresses.

Interpreting changes in quantitative GG scores with regard to improvement or worsening in SSc-ILD is confounded by the fact that GG can transition either to a normal pattern and/or another abnormal pattern (i.e., fibrotic) and that changes in the extent of GG can occur by four different routes (NL→GG, GG→NL, GG→LF or LF→GG). In SLS II, the probability of GG remaining the same was relatively high in both treatment arms (Table 1: 0.50 for whole lung and 0.53 for most severe lobe), but this "stability" appeared to be due to a combination of changes from other patterns of ILD to GG, as well as by concomitant transitions from GG to other patterns. Nonetheless, the clinically important findings were not transitions from LF to GG, but rather the net improvement in response to immunosuppressive therapy was reflected by transitions from either LF or GG to a normal pattern. In addition, these findings indirectly support using reductions in *total* ILD (LF+GG +HC) for the treatment response in contrast to reductions in GG or fibrosis alone [25].

Our findings of a relatively high probability of lung fibrosis transitioning to a normal pattern (compared to the reverse) (0.24 for whole lung and 0.20 for the most severe lobe) (Table 1) are in agreement with the previously reported radiographic results in SLS-I, in which similar probabilities for these transitions in those receiving CYC were observed (0.19 for whole lung and 0.19 for the most severe zone)[21]. Therefore, using two different approaches for quantifying the extent of different patterns of ILD, namely, voxel-wise mapping of volumetric scans in SLS-II and pixel-wise hierarchical mapping using quantitative scores of two-dimensional scans in SLS-I, provided confirmatory findings respecting the partial resolution of lung fibrosis in response to immunosuppressive therapy.

On the other hand, numerically higher probabilities were found in the GG transitions to a normal pattern in the CYC arm of SLS-II (Table 2) compared to the CYC arm of SLS I (0.40 vs. 0.14 respectively, in the whole lung and 0.32, and 0.09, respectively in the most severe lobe and zone at baseline)[21]. This difference might be attributable to the differences between SLS I and SLS II, respectively, in study populations, radiographic techniques (CAD classifier with voxel-wise vs. pixel-wise quantitative scores and segmentation into lobes vs. arbitrarily defined zones), and duration of follow-up (2 years vs. 1 year).

In calculating the probability of these voxel-wise transitional changes, we used a new metric, namely "net improvement" (the results of which are presented in Table 2) to counter potential measurement error in the registration of the two paired HRCT images due to a misalignment in voxels, which could potentially occur in the measurement of both favorable and unfavorable changes. Thus, using the difference of two transitional probabilities would be expected to reduce the impact of possible misalignment from registration.

It is noteworthy that both treatment arms of SLS II demonstrated relatively high probabilities of transitioning from both fibrosis and GG to a normal lung pattern compared with changes in the reverse direction. These observations provide further support for the efficacy of both CYC and MMF in the management of symptomatic SSc-ILD, consistent with the favorable physiologic and patient-centered findings of SLS II, as previously reported [22]. These transitional changes may also provide insights into the pathobiology underlying responses to therapy for SSc-ILD. For example, it is possible that the changes from a ground glass to a normal pattern might represent complete resolution of fine, relatively loosely packed

collagen fibrils, while the changes from a fibrotic to a normal pattern suggests that even coarser, more densely packed collagen is capable of complete resolution. The probability we observed of a net improvement from a fibrotic to a GG pattern was close to zero, implying that the partial resolution of fibrosis in both SLS II and SLS I is reflected predominantly by a transition directly to normal lung rather than by an intermediate pathway wherein coarse fibrosis transitions to a finer sub-resolution type of fibrotic pattern represented by GG. However, it is possible that concomitant changes from GG to a normal pattern may have obscured this intermediate step in the resolution of frank fibrosis.

The results of our analysis should be interpreted within the context of certain limitations. First, the voxel-wise registration between two HRCT scans obtained 2 years apart can be confounded by measurement variation. Second, the metric of probability of changes does not capture the *absolute* extent of the difference in scores for the different patterns (QLF, QGG or QHC), although it does capture the *directional* and proportional changes from baseline within these patterns of ILD. Third, while this metric of the probability of transitional changes in ILD patterns pertains to responses to immunotherapy for SSc-ILD mainly at the group level, its potential usefulness in the assessment and management of individual patients requires further study. Fourth, as with any sensitive computer-aided diagnostic system, standardization, quality control of scanning equipment, methodologies regarding acquisition techniques such as reconstruction kernel, slice thickness, and safe and diagnostic-level of radiation doses are vitally important. Lastly, the transitional changes in ground glass and fibrotic reticulation based on the computer aided classifier model using HRCT lack external validation by tissue histopathology.

SUMMARY AND CONCLUSIONS

Using voxel-by-voxel transitional scores on paired HRCT scans 24 months apart during which patients with SSc-ILD were treated with MMF for the full 2 years or CYC for one year followed by placebo, we observed changes in the extent of ILD patterns indicating comparably significant net transitions from both fibrotic reticulation and ground glass opacity to a pattern of normal lung. These results imply partial resolution of both coarse and fine fibrosis and support and extend previous findings demonstrating improvement in lung function and clinical endpoints in response to treatment with MMF or CYC for SSc-ILD. These findings also demonstrate that voxel-wise changes in ILD patterns of serial HRCT scans may be useful in monitoring the response to treatment of SSc-ILD when other data are inconclusive and provide potential insights into the nature of the therapeutic effects of these two immunosuppressive agents.

Supplementary Material

Refer to Web version on PubMed Central for supplementary material.

Acknowledgement:

Irene Da Costa project manager, Daniel Chong computer programmer, M. Wasil Wahi-Anwar supports 3D rendering plots. Dr. Dinesh Khanna was funded by NIH/ NIAMSR01AR070470.

Grants or other financial supporters of the study: This work was supported by grants from the NHLBI/NIH: R01 HL089758 and R01 HL089901

Abbreviations and acronyms

CYC	Cyclophosphamide
DLCO	carbon monoxide diffusion capacity
FDA	Food and Drug Administration
FVC	Force Vital Capacity
HRCT	High resolution computed tomography
IQR	interquartile range
PFT	Pulmonary Function Test
QGG	Quantitative Ground glass
QHC	Quantitative Honeycomb
QIB	Quantitative Imaging Biomarker
QILD	Quantitative Interstitial Lung Disease, sum of QGG, QLF, and QHC
QLF	Quantitative Lung Fibrosis
QNL	Quantitative Normal Lung
QOL	Quality of Life
MMF	Mycophenolate Mofetil
$\mathbf{P_{NL \rightarrow GG}}$	Proportional changes from normal lung to ground glass, expressed as probability
$\mathbf{P_{NL \rightarrow LF}}$	Proportional changes from normal lung to lung fibrosis, expressed as probability
$\mathbf{P_{NL \rightarrow NL}}$	Proportion remaining as normal lung pattern, expressed as probability
$\mathbf{P_{GG \rightarrow LF}}$	Proportional changes from ground glass to lung fibrosis, expressed as probability
$\mathbf{P_{GG \rightarrow NL}}$	Proportional changes from ground glass to normal lung patterns, expressed as probability
$\mathbf{P_{GG \rightarrow GG}}$	Proportion of remaining as ground glass opacity, expressed as probability
$\mathbf{P_{LF \rightarrow LF}}$	Proportion of remaining as lung fibrosis patterns, expressed as probability

References

1. Abraham DJ, Varga J. Scleroderma: From cell and molecular mechanisms to disease models. Trends Immunol. 2005;26(11):587–595. doi:10.1016/j.it.2005.09.004. [PubMed: 16168711]
2. Hachulla E, Launay D, De Groote P, et al. Severe organ involvement in systemic sclerosis. Reanimation. 2005;14(7):576–586. doi:10.1002/1529-0131(200011)43:11<2437::AID-ANR10>3.0.CO;2-U.
3. Solomon J, Olson AL, Fischer A, Bull T, Brown KK RG. Scleroderma lung disease. Eur Respir Rev. 2014;22(127):6–19. doi:10.1183/09059180.00005512.Scleroderma.
4. Strollo D, Goldin J. Imaging lung disease in systemic sclerosis. Curr Rheumatol Rep. 2010;12(2): 156–161. doi:10.1007/s11926-010-0095-0. [PubMed: 20425026]
5. Steen VD, Conte C, Owens GR, Medsger TA Jr.. Severe restrictive lung disease in systemic sclerosis. Arthritis Rheum. 1994;37(0004–3591 (Print)):1283–1289. [PubMed: 7945490]
6. Hansell DM, Bankier AA, MacMahon H, McLoud TC, Müller NL, Remy J. Fleischner Society: Glossary of Terms for Thoracic Imaging. Radiology. 2008;246(3):697–722. doi:10.1148/radiol.2462070712. [PubMed: 18195376]
7. Kazerooni EA, Martinez FJ, Flint A, et al. Thin-section CT obtained at 10-mm increments versus limited three-level thin-section CT for idiopathic pulmonary fibrosis: correlation with pathologic scoring. Am J Roentgenol. 1997;169(4)(October):977–983. [PubMed: 9308447]
8. Uppaluri R, Heitmman EA, Sonka M, Hartley PG, Hunninghake GW, Mclennan G. Computer Recognition of Regional Lung Disease Patterns. Am J Respir Crit Care Med. 1999;160(2):648–654. doi:10.1164/ajrccm.160.2.9804094. [PubMed: 10430742]
9. Chabat F, Yang G-Z, Hansell DM. Obstructive Lung Diseases: Texture Classification for Differentiation at CT. Radiology. 2003;228(3):871–877. doi:10.1148/radiol.2283020505. [PubMed: 12869685]
10. Zavaletta VA, Bartholmai BJ, Robb RA. High Resolution Multidetector CT-Aided Tissue Analysis and Quantification of Lung Fibrosis. Acad Radiol. 2007;14(7):772–787. doi:10.1016/j.acra.2007.03.009. [PubMed: 17574128]
11. Kim HJ, Li G, Gjertson D, et al. Classification of Parenchymal Abnormality in Scleroderma Lung Using a Novel Approach to Denoise Images Collected via a Multicenter Study. Acad Radiol. 2008;15(8):1004–1016. doi:10.1016/j.acra.2008.03.011. [PubMed: 18620121]
12. Iwasawa T, Asakura A, Sakai F, et al. Assessment of prognosis of patients with idiopathic pulmonary fibrosis by computer-aided analysis of CT images. J Thorac Imaging. 2009;24(3):216–222. doi:10.1097/RTI.0b013e3181a6527d. [PubMed: 19704326]
13. Kim HJ, Tashkin DP, Clements P, et al. A computer-aided diagnosis system for quantitative scoring of extent of lung fibrosis in scleroderma patients. Clin Exp Rheumatol. 2010;28(5 SUPPL. 62). doi:10.1016/j.surg.2006.10.010.Use.
14. Arzhaeva Y, Prokop M, Murphy K, et al. Automated estimation of progression of interstitial lung disease in CT images. Med Phys. 2009;37(1):63–73. doi:10.1118/1.3264662.
15. Marten K, Dicken V, Kneitz C, et al. Interstitial lung disease associated with collagen vascular disorders: Disease quantification using a computer-aided diagnosis tool. Eur Radiol. 2009;19(2): 324–332. doi:10.1007/s00330-008-1152-1. [PubMed: 18726597]
16. Goh NSL, Desai SR, Veeraraghavan S, et al. Interstitial Lung Disease in Systemic Sclerosis. Am J Respir Crit Care Med. 2008;177(11)(December 1999):1248–1254. doi:10.1164/rccm.200706-877OC. [PubMed: 18369202]
17. Leroy EC, Medsger TA. Criteria for the Classification of Systemic Sclerosis (Scleroderma). J Rheumatol. 2001;23(7):1573–1576.
18. Tashkin DP, Elashoff R, Clements PJ, et al. Cyclophosphamide versus Placebo in Scleroderma Lung Disease. N Engl J Med. 2006;354(25):2655–2666. doi:10.1056/NEJMoa055120. [PubMed: 16790698]
19. Roth MD, Tseng CH, Clements PJ, et al. Predicting treatment outcomes and responder subsets in scleroderma-related interstitial lung disease. Arthritis Rheum. 2011;63(9):2797–2808. doi:10.1002/art.30438. [PubMed: 21547897]

20. Kim HJ, Brown MS, Elashoff R, et al. Quantitative texture-based assessment of one-year changes in fibrotic reticular patterns on HRCT in scleroderma lung disease treated with oral cyclophosphamide. Eur Radiol. 2011;21(12):2455–2465. doi:10.1007/s00330-011-2223-2. [PubMed: 21927793]
21. Kim HJ, Tashkin DP, Gjertson DW, et al. Transitions to different patterns of interstitial lung disease in scleroderma with and without treatment. Ann Rheum Dis. 2016;75(7):1367–1371. doi:10.1136/annrheumdis-2015-208929. [PubMed: 26757749]
22. Tashkin DP, Roth MD, Clements PJ, Furst DE, Khanna D, Kleerup EC, Goldin J, Arriola E, Volkmann E R, Kafaja S, Silver R, Steen V, Strange C, Wise R, Wigley F, Mayes M, Riley D J, Hussain S, Assassi S, Hsu VM, Patel B, Phillips K, Martinez F, Golden J, Co ER. Mycophenolate mofetil versus oral cyclophosphamide in scleroderma-related interstitial lung disease (SLS II): a randomised controlled, double-blind, parallel group trial. Lancet Respir Med. 2016;4(9):708–719. [PubMed: 27469583]
23. Mahler DA, Tomlinson D, Olmstead EM, Tosteson AN, O'Connor GT. Changes in dyspnea, health status, and lung function in chronic airway disease. Am J Respir Crit Care Med. 1995;151(1):61–65. doi:10.1164/ajrccm.151.1.7812573. [PubMed: 7812573]
24. Clements PJ, Lachenbruch PA, Seibold JR, et al. Skin thickness score in systemic sclerosis (SSc): an assessment of inter-observer variability in three independent studies. J Rheumatol 1993;20:1892–6. [PubMed: 8308774]
25. Goldin JG, Kim GJ, Brown MB, et al. Longitudinal Changes in Quantitative Interstitial Lung Disease on Computer Tomography after Immunosuppression in the Scleroderma Lung Study II. Ann Am Thorac Soc. 2018 9 28. doi: 10.1513/AnnalsATS.201802-079OC. [Epub ahead of print]
26. Klein S, Staring M, Murphy K, Viergever M a., Pluim J. elastix: A Toolbox for Intensity-Based Medical Image Registration. IEEE Trans Med Imaging. 2010;29(1):196–205. doi:10.1109/TMI.2009.2035616. [PubMed: 19923044]
27. Hoel PG, Port SG, Stone CJ. Introduction to stochastic processes. 1st edn Illinois: Waveland Press Inc., 1987:12–29.
28. Kafaja S, Clements PJ, Wilhalme H, Tseng C-H, Furst DE, Kim GH, et al. Reliability and minimal clinically important difference of FVC results from the Scleroderma Lung Studies (SLS-I and SLS-II). Am J Respir Crit Care Med 2018.
29. Khanna D, Miltoo S, Aggarwal R, et al. Connective Tissue Diseases-associated Interstitial Lung Diseases (CTD-ILD) – Report from OMERACT CTD-ILD Working Group. J Rheumatol. 2015;42(11):3168–2171.
30. Miller MR, Hankinson J, Brusasco V, et al. Standardisation of Spirometry. Eur Respir J. 2005; 26:319–338. [PubMed: 16055882]
31. Graham BL, Brusasco V, Burgos F, et al. 2017 ERS/ATS Standards for Single-breath Carbon Monoxide Uptake in the Lung. Eur Respir J. 2017; 49(1): 1600016.
32. Goh NS, Desai SR, Veeraraghavan S, et al. Interstitial lung disease in systemic sclerosis. A simple staging system. Am J Respir Crit Care Med. 2008;177(11):1248–54. [PubMed: 18369202]
33. Galie N, Hoeper MM, Humbert M, et al. Guidelines for the diagnosis and treatment of pulmonary hypertension: the Task Force for the Diagnosis and Treatment of Pulmonary Hypertension of the European Society of Cardiology (ESC) and the European Respiratory Society (ERS), endorsed by the International Society of Heart and Lung Transplantation (ISHLT). Eur Heart J. 2009;30(20): 2493 [PubMed: 19713419]
34. Volkmann E, Tashkin DP, Sim M, Kim GH, Goldin JG, Clements PJ. Determining progression of scleroderma-related Interstitial Lung Disease: Proceedings of a workshop presented at the 5th World Congress of Systemic Sclerosis, Bordeaux, France, February 2018, J Scleroderma and Related Disorder 2018; doi: 10.1177/2397198318816915journals.sagepub.com/home/jso

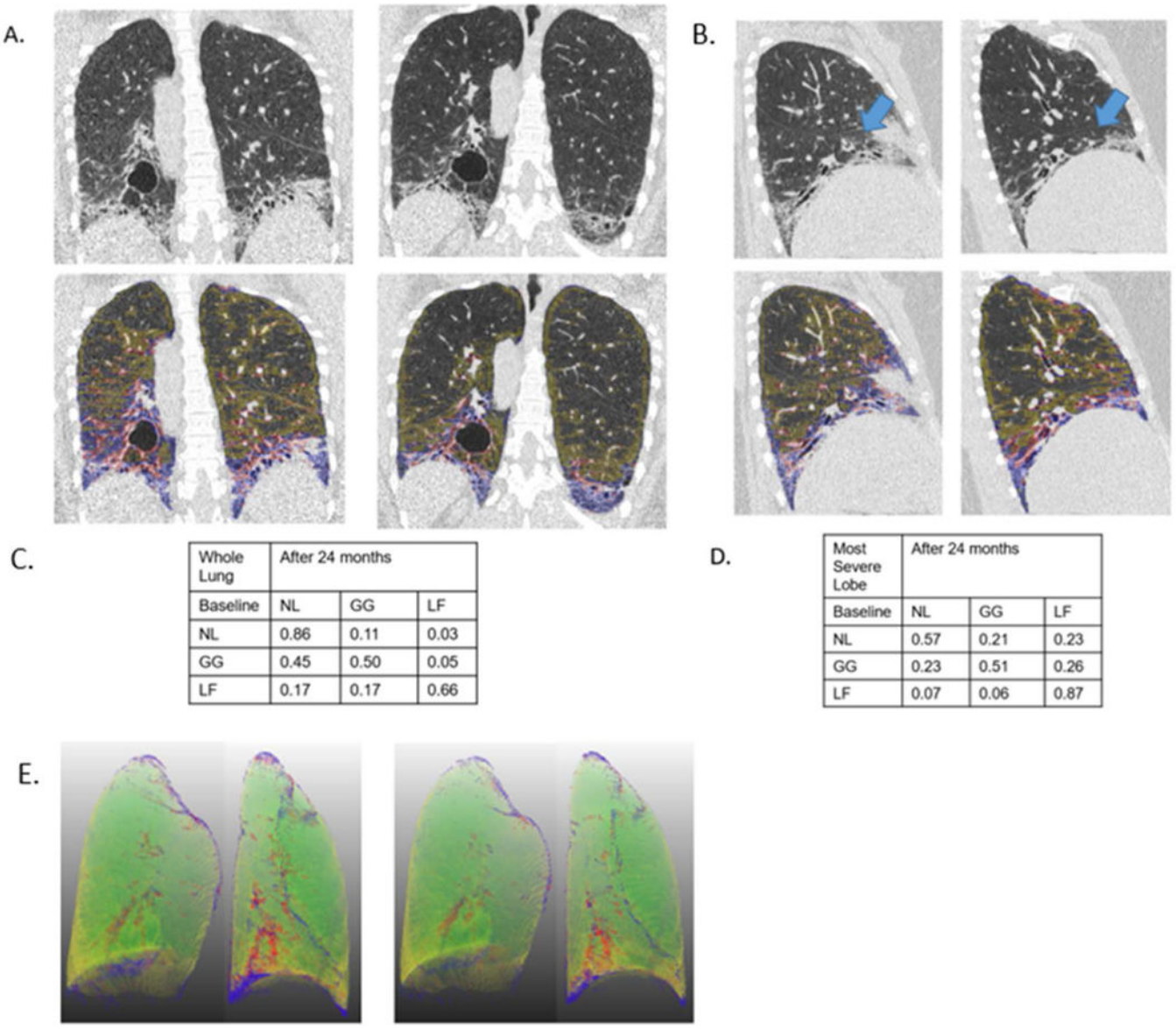

Whole Lung	After 24 months		
Baseline	NL	GG	LF
NL	0.86	0.11	0.03
GG	0.45	0.50	0.05
LF	0.17	0.17	0.66

Most Severe Lobe	After 24 months		
Baseline	NL	GG	LF
NL	0.57	0.21	0.23
GG	0.23	0.51	0.26
LF	0.07	0.06	0.87

Figure 1.

An example of HRCT images with quantitative lung fibrosis score (blue +red overlay) and ground glass score (yellow overlay) on the baseline and 24 month images is shown for a participant assigned to CYC. The rest of the parenchymal area is quantitative normal lung pattern. The 3 rows and 3 columns of the matrix (in tabular form) are the transitional probabilities in this individual subject for whole lung and the most severe lobe (i.e. in this case, the left lower lobe). A. whole lung coronal images; B. sagittal images (blue arrows for right middle lobe); C. whole lung transitional matrix; and D. Most severe lobe (the right middle lobe for this subject) transitional matrix; E. 3D rendering of coronal images for this participant with normal pattern (green), with quantitative lung fibrosis score (blue +red overlay) and ground glass score (yellow overlay).

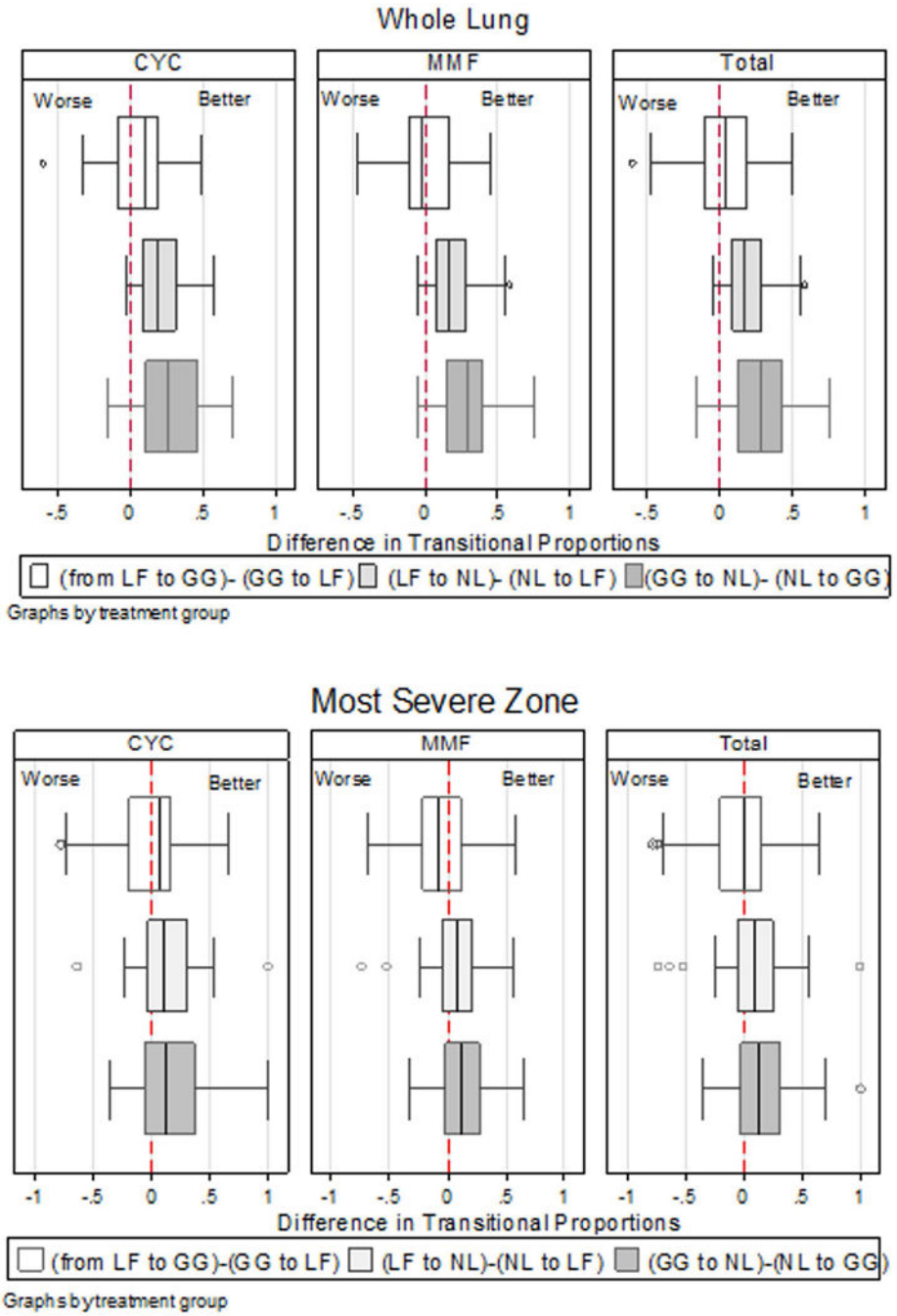

Figure 2.

Box-Whisker plot (median, interquartile range, whisker lines, and outlying points) of proportional changes by treatment arms of cyclophosphamide (CYC) and mycophenolate mofetil (MMF), and the combined group: three changes in the net improvements are expressed in the difference between two proportions, “from lung fibrosis (LF) to ground glass (GG) - GG to LF”, “from lung fibrosis (LF) to normal lung (NL) - NL to LF”, and “from GG to NL – NL to GG”.

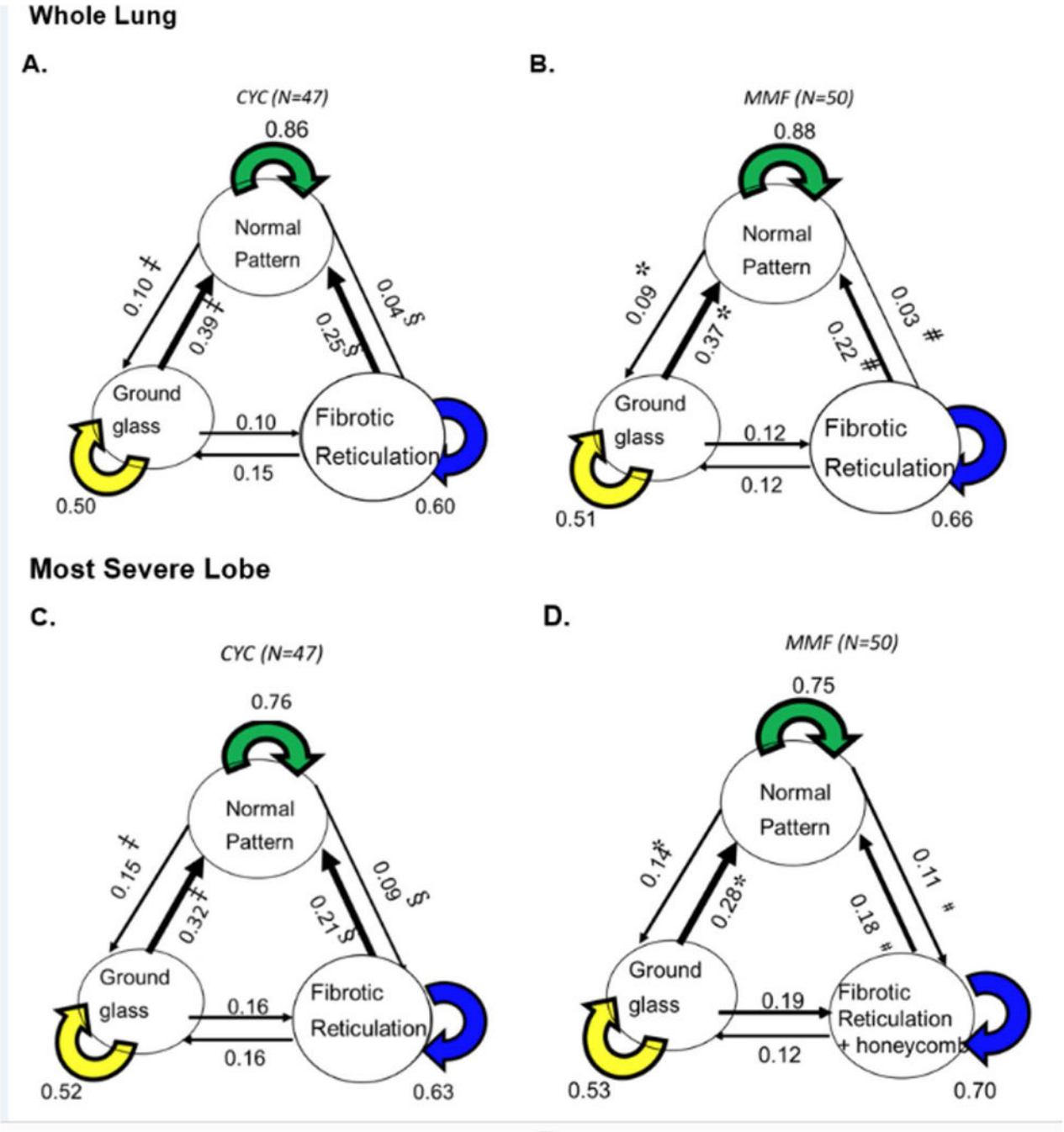

Figure 3.

Schema of transitional matrix by treatment arm: (A) Whole lung in cyclophosphamide (CYC) arm, ‡ p<0.0001, § p<0.0001, and p=0.0568 representing the net improvement between GG and NL patterns, between LF and NL, and between LF and GG, respectively; (B) Whole lung in mycophenolate mofetil (MMF) arm, * p<0.0001, # p<0.0001, and p=0.74 representing the net improvement between GG and NL, between LF and NL, and between LF and GG, respectively; (C) Most severe lobe in CYC arm: ‡ p=0.0008, § p=0.0009, and p=0.87, representing the net improvement between GG and NL, between LF and NL, and

between LF and GG, respectively; (D) Most Severe lobe in MMF arm, *p=0.0002, #p=0.017, and p=0.17 representing the net improvement between GG and NL, between LF and NL, and between LF and GG, respectively.

Table 1.

Probabilities of voxel-wise transitions from one ILD pattern to another by treatment assignment

Whole Lung	*CYC Mean (SE)*			MMF *Mean (SE)*			*Total Mean (SE)*		
Baseline	*NL*	GG	LF	*NL*	GG	LF	*NL*	GG	LF
NL	0.86 (0.02)	0.10 (0.01)	0.04 (0.01)	0.88 (0.01)	0.09 (0.01)	0.03 (<0.01)	0.87 (0.01)	0.10 (0.01)	0.03 (<0.01)
GG	0.40 (0.17)	0.50 (0.15)	0.10 (0.13)	0.37 (0.02)	0.51 (0.02)	0.12 (0.02)	0.38 (0.02)	0.50 (0.01)	0.11 (0.01)
LF	0.25 (0.02)	0.15 (0.02)	0.60 (0.03)	0.22 (0.02)	0.12 (0.01)	0.66 (0.03)	0.24 (0.01)	0.14 (0.01)	0.62 (0.02)
Most Severe Lobe	CYC *Mean (SE)*			MMF *Mean (SE)*			Total *Mean (SE)*		
Baseline	NL	GG	LF	*NL*	GG	LF	*NL*	GG	LF
NL	0.76 (0.03)	0.15 (0.02)	0.09 (0.02)	0.75 (0.03)	0.14 (0.01)	0.11 (0.0)	0.75 (0.02)	0.15 (0.01)	0.10 (0.01)
GG	0.32 (0.03)	0.52 (0.03)	0.16 (0.03)	0.28 (0.03)	0.53 (0.02)	0.19 (0.02)	0.30 (0.20)	0.53 (0.17)	0.17 (0.02)
LF	0.21 (0.03)	0.16 (0.02)	0.63 (0.04)	0.18 (0.02)	0.12 (0.02)	0.70 (0.03)	0.20 (0.02)	0.14 (0.01)	0.66 (0.02)

NL= Normal Lung patterns; GG = Ground Glass patterns; LF = Lung Fibrosis patterns; CYC= Cyclophosphamide; MMF= Mycophenolate Mofetil; Mean and Standard Error (SE) of transitional probabilities ($P_{\text{Baseline}\rightarrow\text{24 month pattern}}$).

Table 2.

Net Improvement in ILD patterns based on voxel-wise transitional changes

Net Improvement	***Whole Lung***		***Most Severe Lobe***	
	CYC Mean (±SE)	***MMF Mean (±SE)***	***CYC Mean (±SE)***	***MMF Mean (±SE)***
$P_{GG\rightarrow NL} - P_{NL\rightarrow GG}$	0.30 (± 0.04)‡	0.28 (±0.03)*	0.17 (±0.05)‡	0.14 (±0.03)*
$P_{LF\rightarrow GG} - P_{GG\rightarrow LF}$	0.05 (±0.03)	0.005 (±0.03)	− 0.006 (±0.04)	− 0.07 (±0.04)
$P_{LF\rightarrow NL} - P_{NL\rightarrow LF}$	0.21(±0.02)†	0.19 (±0.02)$^{\#}$	0.12 (±0.04)†	0.07 (±0.03)$^{\#}$

CYC= Cyclophosphamide; MMF= Mycophenolate Mofetil;

Whole lung:

‡p<0.001;

*p<0.001;

†p<0.001 ;

$^{\#}$p<0.001 ;

Most severe lobe:

‡p=0.0008;

*p=0.0384;

†p=0.0009 ;

$^{\#}$p=0.017 ;

Table 3.

Associations between transitional radiographic changes and baseline characteristics and the changes in lung function, skin score and dyspnea

	Net Improvement					
	Whole Lung			Most Severe Lobe		
	$P_{GG\rightarrow NL}$ - $P_{NL\rightarrow GG}$	$P_{LF\rightarrow GG}$ - $P_{GG\rightarrow LF}$	$P_{LF\rightarrow NL}$ - $P_{NL\rightarrow LF}$	$P_{GG\rightarrow NL}$- $P_{NL\rightarrow GG}$	$P_{LF\rightarrow GG}$ - $P_{GG\rightarrow LF}$	$P_{LF\rightarrow NL}$ - $P_{NL\rightarrow LF}$
Baseline Characteristics : Spearman rank correlation: rho (p-value)						
Male, %	−0.26 (p=0.011*)	−0.24 (p=0.02*)	−0.15 (p=0.14)	−0.24 (p=0.018*)	−0.23 (p=0.024*)	−0.16 (p=0.12)
Age, yr	0.12 (p=0.23)	−0.03 (p=0.74)	−0.09 (p=0.37)	0.15 (p=0.15)	−0.014 (p=0.89)	−0.06 (p=0.56)
Disease Duration	−0.09 (p=0.37)	−0.11 (p=0.30)	−0.17 (p=0.10)	−0.17 (p=0.10)	−0.13 (p=0.19)	−0.10 (p=0.34)
% pred FVC	0.04 (p=0.69)	0.23 (p=0.021*)	0.39 (p=0.0001*)	0.08 (p=0.45)	0.31 (p=0.0024*)	0.38 (p=0.0001*)
FEV1/FVC	−0.24 (p=0.017*)	−0.15 (p=0.14)	−0.20 (p=0.052)	−0.16 (p=0.12)	−0.18 (p=0.077)	−0.17 (p=0.094)
% pred DLCO	0.20 (p=0.0501)	0.23 (p=0.021*)	0.33 (p=0.001*)	0.24 (p=0.02*)	0.25 (p=0.014*)	0.30 (p=0.0025*)
mRSS	−0.07 (p=0.48)	0.11 (p=0.21)	0.15 (p=0.14)	−0.03 (p=0.79)	0.10 (p=0.35)	0.10 (p=0.34)
BDI $^{++}$	0.26 (p=0.011*)	0.14 (p=0.20)	0.22 (p=0.03*)	0.26 (p=0.012*)	0.20 (p=0.049*)	0.25 (p=0.014*)
QLF whole lung,%	−0.29 (p=0.0046*)	−0.37 (p=0.0002*)	−0.67 (p<0.0001*)	−0.32 (p=0.0013*)	−0.49 (p<0.0001*)	−0.71 (p<0.0001*)
QILD whole lung, %	−0.31 (p=0.0018*)	−0.18 (p=0.07)	−0.46 (p<0.0001*)	−0.33 (p=0.0011*)	−0.30 (p=0.0025*)	−0.4881 (p<0.0001*)
QLF Most Severe Lobe, %	−0.30 (p=0.003*)	−0.40 (p=0.0001*)	−0.70 (p<0.0001*)	−0.36 (p=0.0003*)	−0.53 (p<0.0001*)	−0.77 (p<0.0001*)
QILD Most Severe Lobe,%	−0.35 (p=0.0004*)	−0.28 (p=0.0049*)	−0.60 (p<0.0001*)	−0.43 (p<0.0001*)	−0.43 (p<0.0001*)	−0.69 (p<0.0001*)
24 Month Changes: Net Improvement, Spearman rank correlation: rho (p-value)						
	$P_{GG\rightarrow NL}$ - $P_{NL\rightarrow GG}$	$P_{LF\rightarrow GG}$ - $P_{GG\rightarrow LF}$	$P_{LF\rightarrow NL}$ - $P_{NL\rightarrow LF}$	$P_{GG\rightarrow NL}$- $P_{NL\rightarrow GG}$	$P_{LF\rightarrow GG}$ - $P_{GG\rightarrow LF}$	$P_{LF\rightarrow NL}$ - $P_{NL\rightarrow LF}$
Changes in % predicted FVC	0.33 (p=0.0009*)	0.45 (p<0.0001*)	0.21 (p=0.036*)	0.3368 (p=0.0007*)	0.4078 (p<0.0001*)	0.1787 (p=0.0798)
Changes in % predicted DLCO	0.24 (p=0.022*)	0.23 (p=0.028*)	0.08 (p=0.43)	*0.20 (p=0.050)*	0.21 (p=0.042*)	0.14 (p=0.17)
%Changes in TLC	0.28 (p=0.0059*)	0.31 (p=0.002*)	0.21 (p=0.042*)	0.32 (p=0.0017*)	0.29 (p=0.004*)	0.14 (p=0.18)
% Changes in FEV1/FVC	0.02 (p=0.88)	0.03 (p=0.74)	−0.03 (p=0.81)	0.00 (p=1.00)	0.11 (p=0.30)	0.05 (p=0.66)
Change in skin score	−0.107 (p=0.30)	−0.27 (p=0.0066*)	−0.32 (p=0.0016*)	−0.13 (p=0.19)	−0.25 (p=0.014*)	−0.29 (p=0.0043*)
TDI	0.22 (p=0.059)	0.16 (p=0.19)	0.14 (p=0.25)	*0.16 (p=0.18)*	0.09 (p=0.46)	−0.0028 (p=0.98)

% pred = % predicted; FVC = Forced Vital Capacity; FEV1= Forced Expiratory Volume in one second; DLCO = Diffusing capacity of the Lung for carbon monoxide; TLC = Total Lung Capacity; RV = Residual Volume; mRSS = modified Rodnan Skin Score; QLF = Quantitative Lung Fibrosis;

QILD = Quantitative Interstitial Lung Disease= QLF+QGG+QHC= 100%- QNL; BDI = Baseline Dyspnea Index which ranges from 0 (most severe) to 12 (unimpaired). N=97 for changes in skin score: a negative change represents improvement and a positive change represents worsening; N=72 for transition dyspnea index (TDI): a negative change represents worsening and a positive change represents improvement.

[+] N=42 for CYC and N=47 for MMF

[++] N=93 for BDI